HELLENIC REPUBLIC

National and Kapodistrian University of Athens

Department of Biology

Athens International Master's Programme in Neurosciences

Hellenic Pasteur Institute

Laboratory of Cellular and Molecular Neurobiology-Stem Cells

RESEARCH THESIS PROJECT

Astrocytic Dysfunction in Parkinson's Disease: Metabolic Implications of the A53T α-Synuclein Mutation

Tselo Evanthia

Student ID Number: 7113112200009

2023-2024

HELLENIC REPUBLIC
National and Kapodistrian University of Athens
Department of Biology

Athens International Master's Programme in Neurosciences

Hellenic Pasteur Institute

Laboratory of Cellular and Molecular Neurobiology-Stem Cells

RESEARCH THESIS PROJECT

Astrocytic Dysfunction in Parkinson's Disease: Metabolic Implications of the A53T α-Synuclein Mutation

Three Member Evaluation Committee
Supervisor: Dr Papastefanaki Florentia (Research Staff Scientist) Laboratory of Cellular and Molecular Neurobiology, Human Embryonic and Induced Pluripotent Stem Cell Unit, Hellenic Pasteur Institute, Athens, 11521, Greece; fpapastefanaki@pasteur.gr
Thesis reviewer: Dr Taoufik Era (Senior Researcher) Laboratory of Cellular and Molecular Neurobiology, Hellenic Pasteur Institute, Athens, 11521, Greece; etaoufik@pasteur.gr
Thesis reviewer: Thomaidou Dimitra (Research Director) Neural Stem Cells and Neuro-Imaging Group, Hellenic Pasteur Institute, Athens, 11521, Greece; thomaidou@pasteur.gr

2023-2024

Contents

Astrocytic Dysfunction in Parkinson's Disease: Metabolic Implications of the A53T α-Synuclein Mutation

Astrocytic Dysfunction in Parkinson's Disease: Metabolic Implications of the A53T α-Synuclein Mutation

Tselo Evanthia[1,2,3]

[1]Athens International Master's Programme in Neurosciences, Department of Biology, National and Kapodistrian University of Athens, Illisia 15784, Athens, Greece, evacl97@hotmail.com

[2]Laboratory of Cellular and Molecular Neurobiology-Stem Cells, Hellenic Pasteur Institute, Athens, 11521, Greece

[3]Human Embryonic and Induced Pluripotent Stem Cell Unit, Hellenic Pasteur Institute, Athens, 11521, Greece

Supervisor: Papastefanaki Florentia[1,2]

[1]Laboratory of Cellular and Molecular Neurobiology-Stem Cells, Hellenic Pasteur Institute, Athens, 11521, Greece

[2]Human Embryonic and Induced Pluripotent Stem Cell Unit, Hellenic Pasteur Institute, Athens, 11521, Greece, fpapastefanaki@pasteur.gr

Περίληψη

Η Νόσος του Πάρκινσον, η δεύτερη πιο συχνή νευροεκφυλιστική διαταραχή, χαρακτηρίζεται από την απώλεια ντοπαμινεργικών νευρώνων στη μέλαινα ουσία και από την παρουσία ενδοκυτταρικών συσσωματωμάτων της πρωτεΐνης α-συνουκλεΐνης στους νευρώνες, τα οποία ονομάζονται σωμάτια Lewy. Η αυτοσωμική επικρατούσα παθογόνος μετάλλαξη G209A στο γονίδιο *SNCA* που κωδικοποιεί την α-συνουκλεΐνη (p.A53T-αSyn) συμβάλλει στην πρώιμη έναρξη της οικογενούς Νόσου του Πάρκινσον, καθιστώντας την α-συνουκλεΐνη πιο επιρρεπή στη συσσώρευση. Η α-συνουκλεΐνη εκφράζεται κυρίως στους νευρώνες, επομένως η έρευνα έχει επικεντρωθεί σε νευρωνικές δυσλειτουργίες. Ωστόσο, τα αστροκύτταρα, τα κυρίαρχα νευρογλοιακά κύτταρα στον εγκέφαλο, τα οποία παίζουν σημαντικό ρόλο στον ενεργειακό μεταβολισμό μέσω των μιτοχονδρίων τους, εμφανίζουν επίσης συσσωματώματα της πρωτεΐνης α-συνουκλεΐνης. Ωστόσο, μόλις πρόσφατα η έρευνα έχει στραφεί στην συμβολή των αστροκυττάρων στη Νόσο του Πάρκινσον και εξακολουθεί να υπάρχει ένα κενό στην επίδραση της μετάλλαξης p.A53T στο μεταβολισμό τους. Για τη μελέτη της συμβολής αυτής, αξιοποιήσαμε ένα μοντέλο ανθρώπινων επαγόμενων πολυδύναμων βλαστοκυττάρων που φέρουν τη p.A53T μετάλλαξη και τα διαφοροποιήσαμε προς αστροκύτταρα. Τα αποτελέσματά μας έδειξαν μια τάση για αυξημένη κυτταροτοξικότητα και αυξημένα επίπεδα δραστικών ριζών οξυγόνου στα αστροκύτταρα που φέρουν τη μετάλλαξη, τα οποία εμφάνισαν περαιτέρω μια διαταργμένη μιτοχονδριακή μορφολογία, μειωμένη μιτοφαγία και συσσώρευση αποθηκών λιπιδίων (lipid droplets). Τα δεδομένα μας υποδηλώνουν ότι η αστροκυτταρική μιτοχονδριακή και πιθανώς μεταβολική απορρύθμιση μπορεί να συμβάλει στη νευροπαθολογία της Νόσου του Πάρκινσον.

Λέξεις-Κλειδιά

ανθρώπινα επαγόμενα πολυδύναμα βλαστοκύτταρα, αστροκύτταρα, μιτοχόνδρια, μεταβολισμός, λιπίδια

Scientific Summary

Parkinson's Disease (PD), the second most common neurodegenerative disorder, is characterized by progressive loss of dopaminergic neurons in the substantia nigra and by the presence of intraneuronal inclusions of the protein α-synuclein (αSyn), termed Lewy bodies. The autosomal dominant pathogenic G209A mutation in the *SNCA* gene encoding for αSyn (p.A53T-αSyn) contributes to early onset familial PD, by rendering αSyn more prone to aggregation. αSyn is majorly expressed in neurons, therefore research has focused on neuron-intrinsic dysfunctions. However, astrocytes the predominant glial cells in the brain, which play an important role in energy metabolism through their mitochondria, also display intracellular deposits of aggregated αSyn. Yet, it is only recently that research has shifted to the astrocytic contribution in PD and there is still a gap on the effect of the p.A53T mutation in their metabolism. To elucidate this, we leveraged a model of human patient induced pluripotent stem cell-derived p.A53T astrocytes. Our results demonstrated a trend for increased cytotoxicity and elevated levels of reactive oxygen species in p.A53T-αSyn astrocytes, which further displayed an atypical mitochondrial morphology, reflected by a fragmented pattern, impaired mitophagy, and more lipid droplets. Our data suggest that astrocytic mitochondrial and possibly overall metabolic deregulation may contribute to PD neuropathology.

Highlights

- iPSC-derived astrocytes from PD patients with mutant p.A53T-αSyn demonstrate a trend for increased cytotoxicity and elevated ROS levels
- p.A53T-αSyn astrocytes display an atypical mitochondrial morphology, reflected by a fragmented pattern and accompanied by impaired mitophagy
- An accumulation of lipid droplets is observed in p.A53T-αSyn astrocytes, likely indicating disrupted lipid metabolism

Keywords

human, iPSC, astrocytes, mitochondria, metabolism, mitophagy, lipid droplets

Lay Summary

Parkinson's Disease (PD), one of the most common brain diseases, affects 2-3% of the population over the age of 65 and is characterized by both motor symptoms, such as tremor and instability, and non-motor such as constipation, depression, sleep and smell problems. PD is to date incurable, likely due to incomplete understanding of the disease mechanisms, since its research is difficult. Neurons, the main cells of the brain are affected in PD, however astrocytes, a different cell population in the brain, mostly

with supporting role, also play an important part in disease and have attracted researchers' attention for their critical participation in PD. Astrocytes take part in providing the brain with energy, therefore we sought to investigate further their role in PD. To examine this, we used skin cells from both PD patients and healthy people to create patient-specific astrocytes. PD astrocytes displayed problems with their mitochondria, the powerhouse organelles of the cells, and this may imply that they are not able to fulfill their roles as energy providers. Our data suggest that astrocytic problems may contribute to the progression of PD and we anticipate these results will get us one step further in finding a cure for the disease.

Introduction

Parkinson's Disease (PD), the second most common neurodegenerative disorder, affects 2-3% of the population over the age of 65 [1]. Clinically, PD displays both motor symptoms, such as bradykinesia, rest tremor, rigidity and postural instability, and non-motor such as olfactory dysfunction, constipation, depression and REM sleep behavior disorder (RBD) [2]. Pathologically, it is characterized by progressive loss of dopaminergic neurons in the substantia nigra and by the presence of intraneuronal inclusions of the protein α-synuclein (αSyn). These two neuropathological hallmarks are not specific for the disease, but are specific for the definitive diagnosis of it, when applied together [1]. Most PD cases are classified as idiopathic and sporadic, since their etiology is still unknown, and in this instance, aging is considered the major risk factor [3]. Pesticide exposure and traumatic brain injury also attribute to the development of PD, while tobacco smoking and physical activity act as protective factors [4]. However, during the last decades PD onset has been linked to a number of gene mutations. Specifically, 19 genes have been associated with PD, with heterogeneity regarding its phenotype, age-at-onset, and inheritance mode [3]. The most common genes, also accounting for risk factors, include Leucine Rich Repeat Kinase 2-*LRRK2* [5,6], *PARKIN* [7], *GBA* encoding for beta-glucocerebrosidase [8], *DJ-1* [9], and *SNCA* that encodes for α-synuclein [10,11]. The finding of [10] was a breakthrough in PD history, since they identified the first genetic cause, the autosomal dominant pathogenic $SNCA^{G209A}$ mutation driving early onset and severe PD pathology, in a large family from Southern Italy, the "Contursi kindred" and in three smaller families of Greek descent. This point mutation causes the substitution of Alanine-53 by Threonine and results in the expression of the pathological p.A53T-αSyn protein.

Mutations in the *SNCA* gene are responsible for the pathological forms of αSyn and development of PD. However, the physiological function of αSyn is not fully elucidated. It appears that wild type αSyn plays an important role in the Central Nervous System (CNS). It is localized presynaptically [12,13], has been associated with synaptic vesicle trafficking, synaptic function and synaptic plasticity [14,15], and may participate in the regulation of neurotransmitter release [16,17]. αSyn levels depend on the balance between synthesis, aggregation, clearance, and secretion. Any imbalance

between these mechanisms, caused by dysfunction of one or more of these pathways, results in abnormal levels of αSyn and in misfolded αSyn forms [16,18]. The p.A53T point mutation renders αSyn more prone to aggregation and its pathological aggregates can propagate among brain regions and cell populations [16,19,20]. At higher concentrations, p.A53T-αSyn aggregations accumulate and form intraneuronal protein inclusions, termed Lewy bodies (LB) and Lewy neurites (LN), which contribute to the early onset of familial PD [19,21].

In the brain, αSyn is mainly expressed in neurons [16] and to a far lesser extent in glial cells [22]. Its pathological forms have been predominately observed in neurons. However, astrocytes also display intracellular deposits of aggregated αSyn [23]. Specifically, astrocytic αSyn-immunoreactive inclusions were reported in sporadic PD autopsies, exhibiting cortical [22] and nigral distribution [24]. αSyn aggregates in astrocytes cause dysregulations in inflammatory response, in lipid handling and in mitochondrial health and lysosomal function, suggesting that astrocyte dysfunctions could participate in the development and progression of PD pathology [25–27] .

Astrocytes are the predominant glial cells in all areas of the brain and create multiple networks connected by gap junctions [28,29]. Although, they are most known for their role in mediating ionic homeostasis, and providing structural support and passive maintenance for neurons, they also participate in redox homeostasis, in guiding the development and directionality of synapses via release of molecules, such as cholesterol [30–32], in modulating synapse formation and pruning [33], and in regulating transmission efficiency at pre- and post-synaptic sites [34]. In addition, they are involved in promoting neuronal survival through release of neurotrophic factors required for neuronal viability [35], in creating Ca^{2+} signaling networks with neurons and other astrocytes for the control of blood flow and exocytotic release of gliotransmitters [36] and in enwrapping nearly the entire cerebrovasculature creating a physical barrier, the blood brain barrier (BBB) [37]. This structure allows astrocytes to take up molecules from the blood, metabolize them and secrete a range of molecules to other neural cells [29,35,38]. For instance, astrocytes exhibit high glycolytic rates producing lactate, an energy fuel for neurons [39]. Moreover, astrocytes take up glutamate and store fatty acids in lipid droplets to alleviate neuronal cytotoxicity, caused by these metabolites [35,39,40].

Some fundamental astrocyte functions, especially regarding energy metabolism such as those involving fatty acids, are highly dependent on mitochondria [38]. These cell organelles possess their own genome in the form of circular DNA (mtDNA), undergo fusion and fission to regulate their number and morphology, and consist of the outer and inner mitochondrial membrane, separated by the intermembrane space. Most of the mitochondrial functions occur in the inner membrane. Except for their primary role as the powerhouse of the cell, generating ATP through oxidative phosphorylation,

mitochondria also participate in Ca^{2+} homeostasis, the production of endogenous reactive oxygen species (ROS), and in the regulation of apoptosis [41]. Therefore, proper mitochondrial function is important for maintaining the physiological function of astrocytes [42].

Recent data indicate that pathogenic αSyn is involved in astrocytic mitochondrial dysfunction and dysregulated metabolism [42]. For instance, human recombinant αSyn oligomers internalized by human primary astrocytes, localize in mitochondria and cause reduced oxygen consumption [43]. Moreover, exposure of astrocytes to αSyn oligomers reduces ATP levels, disturbs mitochondrial fission–fusion dynamics, and alters mitochondrial morphology, as demonstrated by the presence of fragmented mitochondria [44]. Furthermore, induced pluripotent stem cell-derived astrocytes from PD-patients carrying the *LRRK2*^{G2019S} mutation, including one patient also carrying *GBA*^{N370S} mutation, exhibit abnormal mitochondrial morphology, decreased mitochondrial activity and ATP production, increased production of ROS, and altered metabolism [45,46]. Lastly, postmortem human brain sections from PD patients show astrocytic changes in mitochondrial oxidative phosphorylation protein levels [47]. Hence, emerging data indicate that impaired astrocytic mitochondrial function and metabolism in PD may contribute to the neuropathology of the disease. This drives the interest in researching extensively the contribution of astrocytes in PD, given their critical role in maintaining brain metabolic homeostasis.

In our lab, to elucidate the role of astrocytes in the context of PD, a model of induced pluripotent stem cells (iPSCs) from patients carrying the p.A53T-αSyn mutation and from controls has been developed, including an isogenic pair of p.A53T-αSyn patient and the gene-corrected control. Following established protocols, we differentiated these iPSC lines into ventral midbrain astrocytes. The first results have revealed toxic αSyn accumulation in PD astrocytes and perturbation of major clearance mechanisms, such as the proteasome, autophagy, and the endo-lysosomal pathway (Paschou, Apokotou et al., under submission). Additionally, proteomic analysis of PD astrocytes highlighted a number of differentially expressed proteins related with mitochondrial function and metabolism.

In this work, we hypothesized that the p.A53T mutation affects mitochondrial function and metabolism in astrocytes, which may thereby contribute to PD neuropathology. To address this, we leveraged the model of human patient iPSC-derived p.A53T astrocytes (designated as PDa) and healthy controls (Ha). We addressed the levels of cytotoxicity and ROS in astrocytes, the morphology of mitochondria and the state of mitophagy, and studied the lipid metabolism by examining lipid droplets, fat depots and lipid metabolism regulators.

Methods

Differentiation of Neural Progenitor Cells into Astrocytes

The iPSCs used for generating the neural progenitor cells (NPCs) included lines from two male PD patients (PD1 and PD2) carrying the G209A (p.A53T) *SNCA* mutation and one age- and sex-matched non-PD subject (H1), previously generated in our lab [48], an age- and sex-matched non-PD control line (H2) obtained from the New York Stem Cell Foundation, a female PD iPSC line (PD3) carrying the G209A *SNCA* mutation and its gene-corrected isogenic control line ($PD3^{corr}$) [49] **(Table 1)**. Differentiations from independent non-isogenic iPSC clones were considered biological replicates [H1.1, H1.2, H1.3, H2 for the control (non-PD) condition and PD1.1, PD1.2, PD2.1, PD2.2 for the PD condition] and the outcome was separately validated in the isogenic pair (PD3 vs $PD3^{corr}$). Following iPSC neuralization via dual SMAD inhibition and by using established protocols [50,51], ventral midbrain-patterned NPCs were obtained. Only those NPCs that passed the quality control for their regionalization were used for differentiation into astrocytes.

Ventral midbrain NPCs were differentiated into astrocytes, by using a protocol (28 days) described by Aurelie de Rus Jacquet [51], based on the previously published methodology for the production of astrocytes from forebrain NPCs using a ready-to-use medium, commercially available by ScienCell Research Laboratories [52]. To initiate differentiation, midbrain-patterned NPCs (after at least 4 weeks of expansion in NPC medium) were plated at 15,000 cells/cm^2, continuously maintained in astrocyte differentiation medium (AM, Sciencell Research Laboratories), and passaged approximately every 7 days until day 28. In addition, this medium requires supplementation with 2% Fetal Bovine Serum (FBS), which may affect downstream applications. The growth rate of different NPC lines may vary, especially during the first 14 days of differentiation, meaning that the plating density and the passaging schedule may require adaptation depending on the line. Cell morphology was a visual indicator of differentiation and was progressively changed. Small round NPCs gave rise to large, flat astrocytes. Both NPCs and iPSC-derived astrocytes are cryopreserved in Bambanker freezing medium (Nippon Genetics).

Table 1. Summary of patient-derived cell lines used in this study

	Donor status	iPSC line coding	Age at biopsy	αSyn mutation	Sex	Source/reference
Non-isogenic	Healthy (non-PD control)	H1.1	41	Wild Type *SNCA*	M	[48]
		H1.2				
		H1.3				
	Healthy (non-PD control)	H2	45	Wild Type *SNCA*	M	New York Stem Cell Foundation
	Parkinson's Disease Patient	PD1.1	49	G209A *SNCA*	M	[48]
		PD1.2				
	Parkinson's Disease Patient	PD2.1	40	G209A *SNCA*	M	[48]
		PD2.2				

Isogenic pair	Parkinson's Disease Patient	PD3	49	G209A *SNCA*	F	[49]
	Parkinson's Disease Patient (gene-corrected control)	$PD3^{corr}$	49	G209A *SNCA* corrected	F	[49]

Maturation of Astrocytes

After the 28-day differentiation protocol, morphological and functional characterization showed that the induced astrocytes are immature. Previous data have shown that astrocytes perform diverse functions depending on their developmental stage [53]. It is known that immature astrocytes support neuronal maturation while when they mature, they focus on CNS homeostasis, such as trophic and metabolic support to neurons and BBB regulation (Lattke and Guillemot, 2022). Therefore, it was important to perform some experiments on both immature and mature astrocytes, since maturation state affects their role, it may also affect their contribution to PD progression. For that reason, astrocytes were kept in culture and treated for maturation. Particularly, they were plated at 30,000 cells/well on Geltrex-coated glass coverslips in 48-well plate and on day 0 of the maturation protocol AM was switched to Astro-Maturation Medium (1:1 Advanced DMEM/F-12, 2% B27 without vitamin A, 1% Glutamax, 1% N2 and 1% Non-Essential Amino-Acids) plus Bone-Morphogenetic Protein-4 and Ciliary Neurotrophic Factor (BMP4, CNTF both 20 ng/μL, Peprotech). The maturation period lasted for at least 2 weeks, with medium changes every other day. In addition, for the first 7 days of maturation the cells were treated with 0.5% FBS, which afterwards was fully withdrawn.

Extracellular LDH activity as a measurement for cytotoxicity

LDH is an enzyme present in almost all body tissues and catalyzes the conversion of pyruvate to lactate and back. Its abundance is indicative of plasma membrane damage in a cell population, since it is released from the cytosol of the damaged cells to the supernatant. LDH activity was assayed on p.A53T-αSyn astrocytes and their controls. Differentiation day-28 immature astrocytes were plated at 20,000-25,000 cells/well, depending on the proliferation rate of each line, on Geltrex-coated glass coverslips in 48-well plates in AM. After 1 day, FBS was removed from the medium. FBS is usually removed from the cell culture medium, before performing different assays mainly for 2 reasons. Firstly, to synchronize the cells to the same cell cycle phase and secondly, to avoid interaction of growth factors, lipids, hormones, and additional nutrients found in FBS with components of the assay, which may affect the assay's outcome [54]. Therefore, 24 and 48 hours after removing FBS from the culture medium, supernatants were collected and assayed according to the manufacturer's instructions [Cytotoxicity Detection Kit (LDH), Roche]. At the same time, the glass coverslips containing the cells were fixed with 4% paraformaldehyde (Sigma-Aldrich) in PBS for 15 min at 22-23°C, mounted with StayBrite Hardset Mounting Medium with DAPI (Biotium) and were let dry for 16 hours, at 22-23 °C in the dark. Images of these cells

were acquired using a Leica TCS-SP8P confocal microscope (LEICA Microsystems) with a 20X objective. The purpose of this imaging is the cell number measurement of each coverslip for the normalization of the respective LDH activity result.

Immunofluorescence

To analyze immature and mature astrocytes by immunofluorescence, cells were plated on Geltrex-coated glass coverslips at medium to high confluency and were fixed with 4% paraformaldehyde (Sigma Aldrich) in PBS for 15 min at 22-23 °C. Afterwards, they were blocked for 15 min with 0.1% Triton X-100 (Sigma-Aldrich) in PBS, then permeabilized (for intracellular epitopes) with 5% normal donkey serum in PBS and subsequently incubated with primary antibodies **(Table 2)** at 4 °C for 16-18 hours, followed by incubation with the appropriate combination of secondary antibodies (Thermo Fisher Scientific) conjugated with AlexaFluor-488, -546, or -647 for 2 hours at 22-23 °C. Coverslips after 3 washes with PBS and one with ddH_2O, were mounted with StayBrite Hardset Mounting Medium with DAPI (Biotium) and were let dry for 16 hours, at 22-23 °C in the dark before proceeding with confocal imaging. Images were acquired using a Leica TCS-SP5II confocal microscope (LEICA Microsystems) with a 63X oil immersion objective and 1.5 zoom.

Table 2. Primary Antibodies

Epitope	Manufacturer	Catalog Number	Dilution
LAMP1	Developmental Studies Hybridoma Bank, Iowa City, IA, USA	H4A3-s	1/100
VIMENTIN	Synaptic Systems, Goettingen, Germany	172006	1/500
TOMM20	Santa-Cruz Biotechnology	sc-11415	1/200

Reactive Oxygen Species (ROS) detection

For ROS measurement in live immature astrocytes, the Celldiscoverer 7 imaging system (Zeiss, Oberkochen, Germany) was used. Immature astrocytes were plated at 20,000- 25,000 cells/well in Geltrex-coated glass bottom 8-well plates (Ibidi) in AM and one day before the assay FBS is removed from the medium. The day of the experiment, Ha and PDa with similar densities were selected, washed once with HBSS, incubated with 5μM DCFDA (Abcam, Cambridge, UK) and 0.3μM MitoTracker™ Red CMXRos (Thermo Fisher Scientific) in HBSS for 25 min at 37 °C, 5% CO_2 and >70% humidity. Then, the cells were washed twice and equilibrated in HBSS for 10 min in the microscope's environmental chamber (same conditions as the incubation). Images were acquired by a confocal setup with a 50X water immersion objective at 488 nm for DCFDA and 594 nm for MitoTracker™ Red CMXRos.

Detection of Lipid Droplets

For assessing lipid droplets in the immature astrocytes, cells were plated at 20,000 cells/well on Geltrex-coated glass coverslips in 48-well plates in AM. One day before the assay, FBS was removed from the cell culture medium. The day of the assay, cells

were washed once with HBSS, incubated with 0.5 μg/mL NileRed (Thermo Fisher Scientific) in HBSS for 5 min at 37 °C, 5% CO_2 and >70% humidity. Then, they were washed twice with HBSS, fixed with 1% paraformaldehyde (Sigma Aldrich) in PBS for 15 min at 22-23 °C, mounted with StayBrite Hardset Mounting Medium with DAPI (Biotium) and were let dry for 16 hours, at 22-23 °C in the dark before confocal imaging. Images were acquired using a Leica TCS-SP8P confocal microscope (LEICA Microsystems) with a 63X oil immersion objective and 1.5 zoom at 552 nm.

Table 3. Reagents used in this study

Reagents	Company	Catalog Number
DCFDA	Abcam, Cambridge, UK	ab113851
DMEM High Glucose w/ L-Glutamine w/ Sodium Pyruvate	Biosera, Nuaille, France	LM-D1111/500
Hanks' Balanced Salts Solution w/o Ca w/o Mg w/o Na Bicarbonate w/o Phenol Red (HBSS)	Biosera, Nuaille, France	LM-S2034/500
StayBrite Hardset Mounting Medium with DAPI	Biotium, Fremont, CA, USA	23004
BMP4	Peprotech, Cranbury, NJ, USA	AF-120-05ET-B
CNTF	Peprotech, Cranbury, NJ, USA	450-13-B
EGF	Peprotech, Cranbury, NJ, USA	GMP100-15
FGF-Basic (146 a.a.) Human Recombinant (FGF-2)	Peprotech, Cranbury, NJ, USA	100-18C-0100
Astrocyte Medium (AM)	ScienCell Research Laboratories, Carlsbad, CA, USA	1801
Cytotoxicity Detection Kit (LDH)	Sigma Aldrich, St. Louis, MO, USA	11644793001
Paraformaldehyde	Sigma Aldrich, St. Louis, MO, USA	30525-89-4
Triton™ X-100	Sigma Aldrich, St. Louis, MO, USA	9036-19-5
Advanced DMEM/F12	Thermo Fisher Scientific, Waltham, MA, USA	12634010
B-27™ Supplement (50X), minus vitamin A	Thermo Fisher Scientific, Waltham, MA, USA	12587-010
Fetal Bovine Serum (FBS)	Thermo Fisher Scientific, Waltham, MA, USA	10270-106
Geltrex LDEV FREE HESC QUAL	Thermo Fisher Scientific, Waltham, MA, USA	A1413302
GlutaMAX (100X)	Thermo Fisher Scientific, Waltham, MA, USA	35050-038
HAM's F12	Thermo Fisher Scientific, Waltham, MA, USA	21765-029
HEPES 1M	Thermo Fisher Scientific, Waltham, MA, USA	15630-106
MEM Non-Essential Amino Acids Solution (100X)	Thermo Fisher Scientific, Waltham, MA, USA	11140-035
MitoTracker™ Red CMXRos	Thermo Fisher Scientific	M7512
N-2 Supplement (100X)	Thermo Fisher Scientific, Waltham, MA, USA	17502-048
Neurobasal™ Medium	Thermo Fisher Scientific, Waltham, MA, USA	21103-049

Nile Red	Thermo Fisher Scientific	N1142
Penicillin/Streptomycin	Thermo Fisher Scientific, Waltham, MA, USA	15140-122
Phosphate-Buffered Saline, pH 7.4	Thermo Fisher Scientific	10010-015
StemPro® Accutase	Thermo Fisher Scientific, Waltham, MA, USA	A1110501
Y-27632 ROCK inhibitor	Tocris, Bristol, UK	1254
Bambanker	Nippon Genetics, Düren, Germany	BB02

Advanced Image Analysis

All image analyses were performed on FIJI (NIH).

Mitochondrial Morphology Analysis

Mitochondrial Morphology (number, size, sphericity) was analyzed through the "Mitochondria Analyzer" plugin [55]. To use this plugin, images were first deconvolved. For the deconvolution process, a PSF (Point Spread Function) is necessary. Therefore, a theoretical PSF was generated, by using the "PSF Generator" plugin [56] and specifically the "Gibson & Lanni 3D Optical Model" algorithm. PSF was generated based on the microscope parameters and image properties, and this specific algorithm was chosen as the most accurate one, since detailed information is needed for the PSF generation. Then, deconvolution was performed with the "Deconvolution Lab2" plugin, utilizing the Richardson-Lucy algorithm with maximum iterations of 30 [57,58]. Before deciding on this algorithm and iterations, several trials were carried out with different parameters for the most accurate choice.

The deconvolved 3D images were then processed using the "Mitochondria Analyzer" plugin. First, these images were converted to 8-bit, a necessary step for using the plugin. Afterwards, by utilizing the "3D Threshold" command of the plugin the 3D images were pre-processed, thresholded and post-processed according to the extensive analysis of [55]. In the thresholding section, different methods and parameters could be used, but the most precise ones for our images were the "weighted mean" method with block size "1.25 microns" and c-value "3". Lastly, "3D analysis" command was used in the final 3D processed images and the results were obtained.

LAMP1 Staining Analysis

The number and size of LAMP1$^+$ puncta were counted using the "Analyze Particles" plugin and cell area was considered as region of interest (ROI). In this plugin, the size in square microns was set between 0.2-4.5 and the circularity between 0.2-1. Before that, a pre-processing macro of commands was created as outlined next and applied to the images.

"run("8-bit");
run("Median...", "radius=2 stack");
run("Z Project...", "projection=[Max Intensity]");

run("Bandpass Filter...", "filter_large=7 filter_small=3 suppress=None tolerance=5 autoscale saturate");
run("Auto Threshold", "method=Intermodes white");
run("Watershed");
run("Fill Holes");"

TOMM20 and LAMP1 Colocalization Analysis

To determine the level of colocalization, the JACoP (BIOP Version) plugin with Manders coefficients was used. "Moments" auto threshold was applied on z-stack of both channels/proteins before measuring and the cell area was considered as ROI.

ROS levels Analysis

ROS levels based on DCFDA and on MitoTracker™ Red CMXRos labeling were measured as Mean Grey Value per cell, using constant auto threshold settings and considering each cell area as ROI. For better presentation of the results in the graphs, each value (Ha and PDa) is portrayed divided by the mean of the Ha values.

Lipid Droplet Analysis

The cell area covered by lipid droplets is defined as the area of the ROI (cell) where NileRed staining is present. "Max Entropy" auto threshold was applied beforehand.

The number and size of lipid droplets based on NileRed labeling were counted using the "Analyze Particles" plugin and the cell area was considered as ROI. In this plugin, the size in square microns was set between 0.2-20 and the circularity between 0.2-1. Before that, a pre-processing macro of commands was created and applied in the images.

"run("Median...", "radius=2 stack");
run("Z Project...", "projection=[Max Intensity]");
run("Bandpass Filter...", "filter_large=10 filter_small=3 suppress=None tolerance=5 autoscale saturate");
run("Auto Threshold", "method=Intermodes white");
run("Fill Holes");"

Statistical Analysis

All experiments were performed in at least 3 biological replicates of healthy and PD samples. In most experiments non-isogenic lines were examined separately from the isogenic pair, used to verify the causality of the mutation, unless otherwise stated. For each readout, the exact details of analysis and statistics are given in figure legends. Statistical analysis was performed in GraphPad Prism (San Diego, CA, USA) and p-value for significance was set to ≤ 0.05.

Results

p.A53T-αSyn astrocytes show a trend for increased cytotoxicity

First, we wanted to investigate whether the p.A53T-αSyn mutation affects cell viability of the PD-patient iPSC-derived astrocytes. Previously, it has been shown that accumulation of αSyn causes increased cytotoxicity [43]. For this reason, Lactate Dehydrogenase (LDH) activity was measured in the supernatants, which indicates plasma membrane damage in a cell population.

LDH activity measurement was performed in immature p.A53T-αSyn astrocytes and controls at two time points, 24 and 48 hours after removing FBS from their culture medium. We observed a trend for elevated LDH release in PDa in both time points **(Figure 1A, B)**. However, these results did not reach statistical significance, possibly due to high variance between the cell lines that are derived from different donors **(Table 1)**. Nevertheless, increased LDH activity in PDa suggests that the p.A53T mutation can lead to increased cytotoxicity in astrocytes and subsequently affect their function.

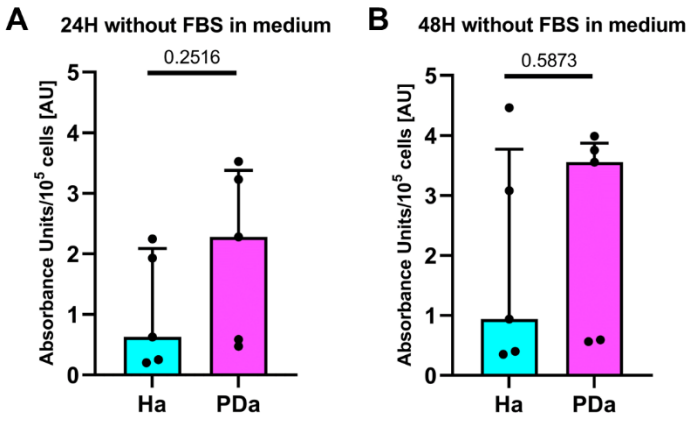

Figure 1. A trend for increased cytotoxicity displayed in the p.A53T-αSyn astrocytes.
Bar Plots representing absorbance units at 490 nm of Lactate Dehydrogenase substrate in cell supernatants from immature Ha and PDa. Data were acquired (A) 24 hours and (B) 48 hours after removing FBS from the culture medium of the cells and are presented as median with interquartile range. Each dot represents the mean of triplicate absorbance measurement of a biological replicate (n = 5, 4 non-isogenic lines and 1 isogenic pulled together), normalized per cell number (per 10^5 cells). Unpaired t-test with Welch's correction was used for comparisons and p-values are shown on the graphs.
Ha: Healthy Astrocytes, PDa: p.A53T-αSyn astrocytes, H: hours, FBS: Fetal bovine serum, AU: Absorbance Units

p.A53T-αSyn astrocytes exhibit a trend of abnormal mitochondrial morphology, including fragmented mitochondria

Mitochondria are important cell organelles, particularly in the nervous system, as they dynamically migrate, divide, and fuse. Cycles of mitochondrial fission and fusion ensure metabolite and mitochondrial DNA mixing and establish their shape, number and bioenergetic functionality. Disruption of this cable-like morphology of functional mitochondria leads to impaired bioenergetics and mitochondrial migration, and can

trigger neurodegeneration [59]. Previous studies have shown abnormalities in mitochondrial morphology, specifically fragmentation of mitochondria in iPSC-derived astrocytes from PD-patients carrying the *LRRK2*^{G2019S} mutation [45] and reduced fission in DJ-1 knockdown primary astrocytes [60], Hence, we wanted to explore whether the p.A53T-αSyn mutation also affects mitochondrial morphology in astrocytes, that could eventually contribute to PD neuropathology. To address this, we performed immunostaining for TOMM20, a protein found in the outer mitochondrial membrane, in immature and mature PD-patient iPSC-derived astrocytes and healthy controls. High power confocal microscopy and advanced image analysis were employed.

While immature healthy astrocytes contained elongated and interconnected mitochondria, PD astrocytes contained smaller **(Figure 2A, C, F)** and more spherical **(Figure 2A, D, G)** mitochondria**,** indicating increased fragmentation **(Figure 2A)**. However, only the isogenic pair reached statistical significance, probably because of elimination of potential variations due to different genetic backgrounds present among the non-isogenic lines **(Figure 2E-G)**. Regarding the number of mitochondria per cell **(Figure 2B, E)**, there was a deviation between the results obtained by the analysis of the isogenic pair as compared to those obtained from the non-isogenic lines. In the latter, the number of mitochondria in PDa is decreased, while in the isogenic pair, PD astrocytes contain more mitochondria than their controls. Since both results reached statistical significance, additional experiments should be conducted to reach a safe conclusion.

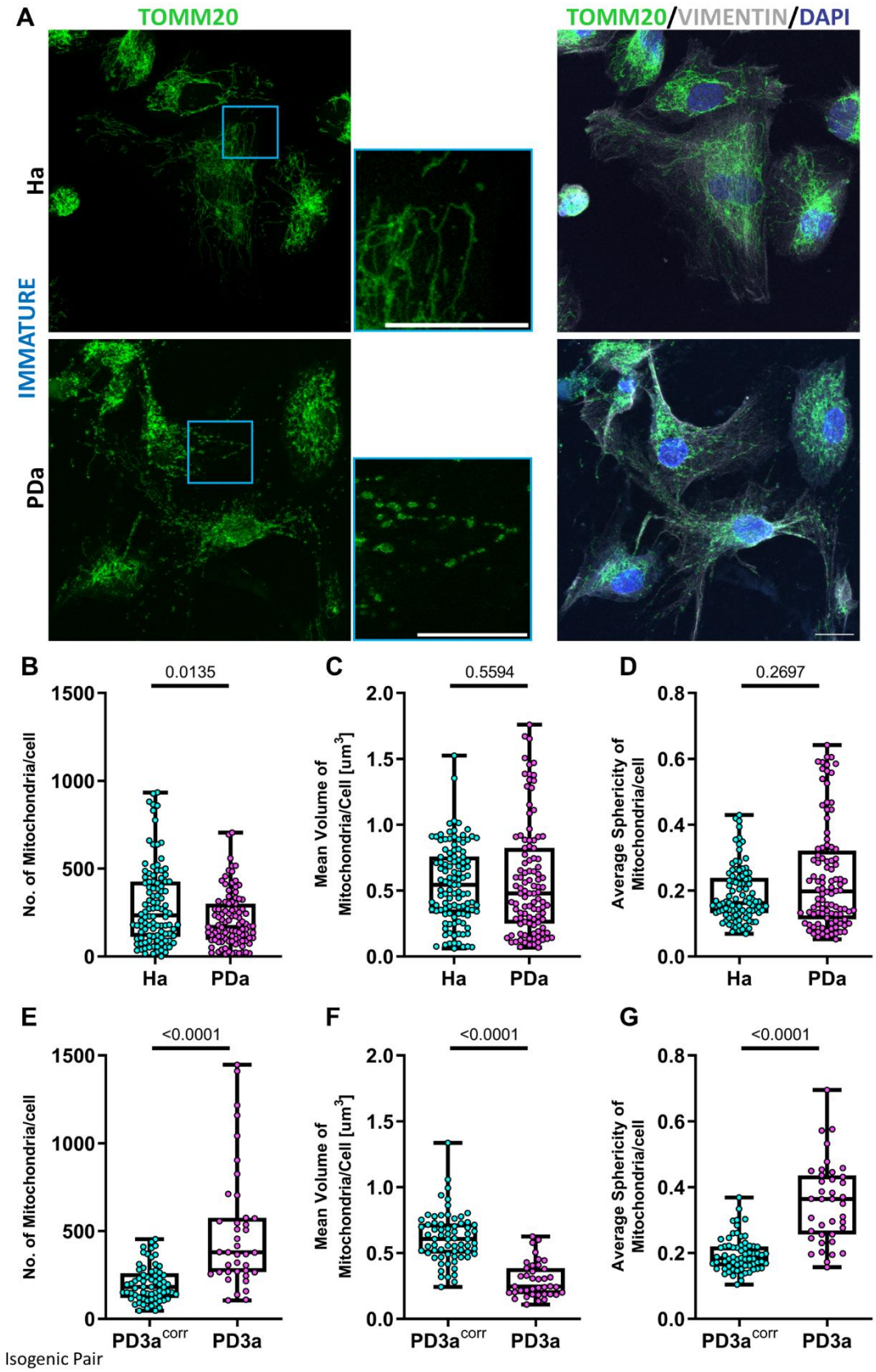

Figure 2. Mitochondrial abnormalities in immature p.A53T-αSyn astrocytes.

A: Representative confocal images of immature Ha and PDa immunostained for TOMM20, and VIMENTIN, with DAPI. Insets show magnified views of boxed regions. Scale bar: 20 µm.

B-G: Box and whiskers plots showing the distribution of the number of mitochondria in non-isogenic (B) and isogenic lines (E), of the mean volume of mitochondria in non-isogenic (C) and isogenic lines (F) and

of the average sphericity of mitochondria in non-isogenic (D) and isogenic lines (G). Data are presented as median with interquartile range and min and max values, and each dot represents a cell. Mann-Whitney tests were used for comparisons and p-values are shown on the graphs. Sample sizes: B: n = 106 Ha and n = 99 PDa across 4 non-isogenic Ha lines and 4 non-isogenic PDa lines, C: n = 111 Ha and n = 105 PDa across 4 non-isogenic Ha lines and 4 non-isogenic PDa lines, D: n = 96 Ha and n = 100 PDa across 4 non-isogenic Ha lines and 4 non-isogenic PDa lines, E, F, G: n = 68 PD3a^{corr} and n = 39 PD3a.
TOMM20: Translocase of Outer Mitochondrial Membrane 20, Vimentin: Intermediate Filament Protein, DAPI: 4',6-diamidino-2-phenylindole, Ha: healthy astrocytes, PDa: p.A53T-αSyn astrocytes, PD3a: p.A53T-αSyn astrocytes, PD3a^{corr}: Corrected isogenic astrocytes

Mature astrocytes showed a similar trend to that of the immature ones. PDa contained more mitochondria **(Figure 3A, B, E)**, smaller in size **(Figure 3A, C, F)**, and more spherical thus rather fragmented **(Figure 3A, D, G)**. However, only the isogenic pair reached statistical significance.

Less, smaller, and spherical mitochondria indicate mitochondrial fragmentation and dysfunction in the processes of fusion or fission [59]. In our case, there was a trend for increased fragmentation, indicating decreased fusion or increased fission in both immature and mature PDa.

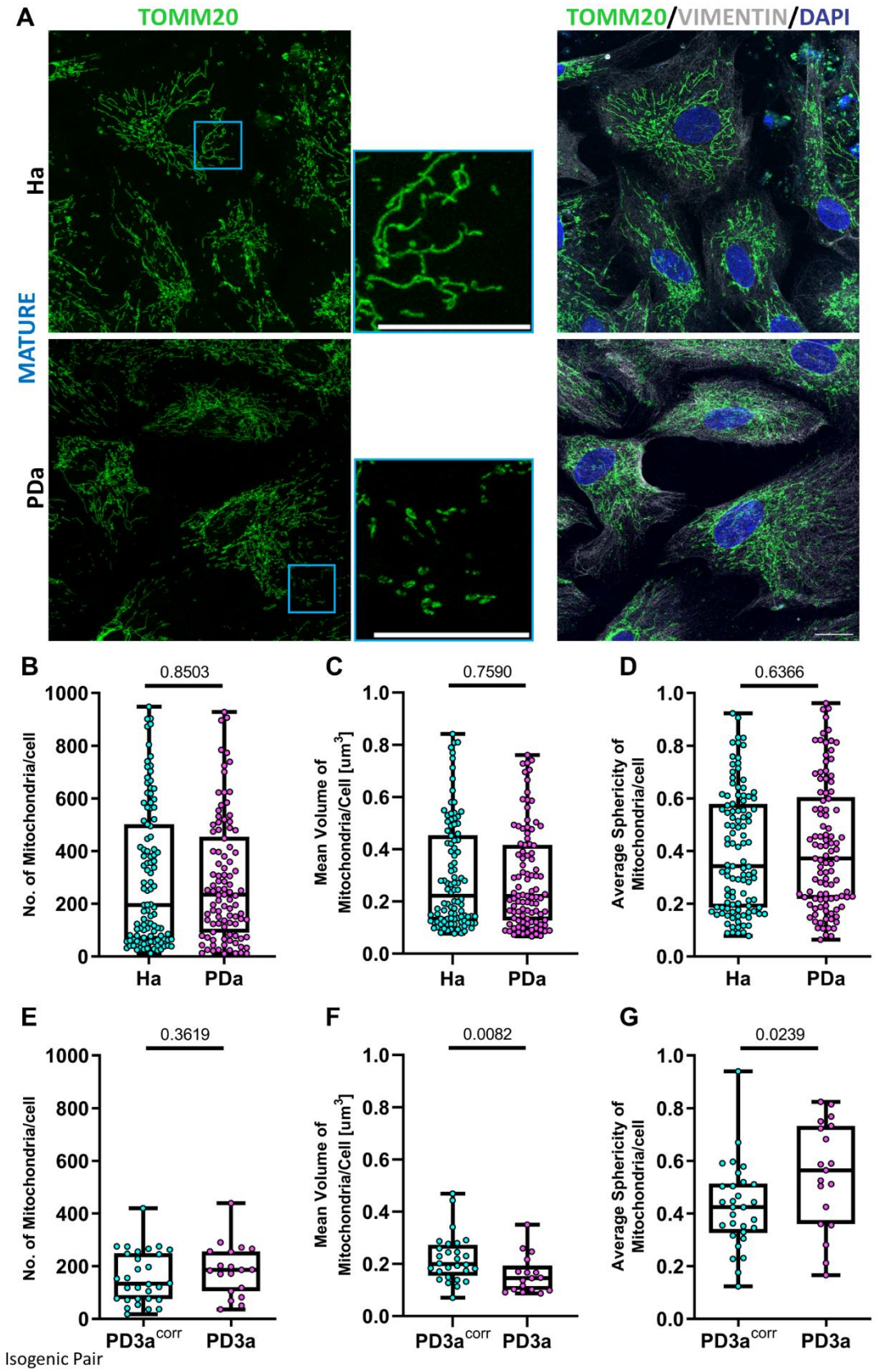

Figure 3. Mitochondrial abnormalities in mature p.A53T-αSyn astrocytes

A: Representative confocal images of mature Ha and PDa immunostained for TOMM20, and VIMENTIN, with DAPI. Insets show magnified views of boxed regions. Scale bar: 20 µm.

B-G: Box and whiskers plots showing the distribution of the number of mitochondria in non-isogenic (B) and isogenic lines (E), of the mean volume of mitochondria in non-isogenic (C) and isogenic lines (F),

and of the average sphericity of mitochondria in non-isogenic (D) and isogenic lines (G). Data are presented as median with interquartile range and min and max values, and each dot represents a cell. Mann-Whitney tests were used for comparisons and p-values are shown on the graphs. Sample sizes: B: n = 107 Ha and n = 98 PDa across 4 non-isogenic Ha lines and 4 non-isogenic PDa lines, C: n = 102 Ha and n = 99 PDa across 4 non-isogenic Ha lines and 4 non-isogenic PDa lines, D: n = 107 Ha and n = 102 PDa across 4 non-isogenic Ha lines and 4 non-isogenic PDa lines, E, G: n = 30 PD3a^{corr} and n = 19 PD3a, F: n = 28 PD3a^{corr} and n = 17 PD3a.
TOMM20: Translocase of Outer Mitochondrial Membrane 20, Vimentin: Intermediate Filament Protein, DAPI: 4',6-diamidino-2-phenylindole, Ha: healthy astrocytes, PDa: p.A53T-αSyn astrocytes, PD3a: p.A53T-αSyn astrocytes, PD3a^{corr}: Corrected isogenic astrocytes

Indications for disturbed mitophagy in the p.A53T-αSyn astrocytes

The combination of increased cytotoxicity along with the presence of mitochondrial fragmentation led us to examine the clearance of mitochondria. This is accomplished by a selective form of autophagy, called mitophagy [61]. In autophagy, cell components are non-selectively enveloped in a double-membrane structure called autophagosome, which is then fused with lysosomes for degradation [61,62]. In mitophagy, mitochondria are engulfed in the autophagosome [61]. Mitochondria-lysosome membrane contact sites are very important for the proper function of mitophagy [63]. Therefore, we sought to address whether the interaction between these two organelles is altered in PDa due to the p.A53T-αSyn mutation. To explore this interaction, we first performed immunocytochemistry for LAMP1 (Lysosomal-associated membrane protein 1), a transmembrane glycoprotein located at the lysosomal membrane with crucial roles in maintaining lysosomal integrity and function [64]. We analyzed LAMP1$^+$ lysosomes in immature and mature p.A53T-αSyn astrocytes and their controls, and then examined the colocalization between LAMP1 and TOMM20, by high power confocal microscopy and exhaustive image analysis.

<u>Assessment of lysosomal number and size</u>

In immature PD astrocytes the number of LAMP1$^+$ puncta was increased compared to the healthy controls **(Figure 4A, B)**. The isogenic pair was in accordance with the non-isogenic lines, since PD3a also exhibited a statistically significant increase of LAMP1$^+$ puncta, as compared to their gene-corrected controls PD3a^{corr} **(Figure 4D**). On the other hand, the size of LAMP1$^+$ puncta did not differ between PDa and their controls in neither the non-isogenic or isogenic lines **(Figure 4C, E).** The increase of LAMP1$^+$ puncta in immature PDa, reflects an increase in the number of lysosomes, indicating that PDa may have heightened need in using the lysosomal degradation pathways.

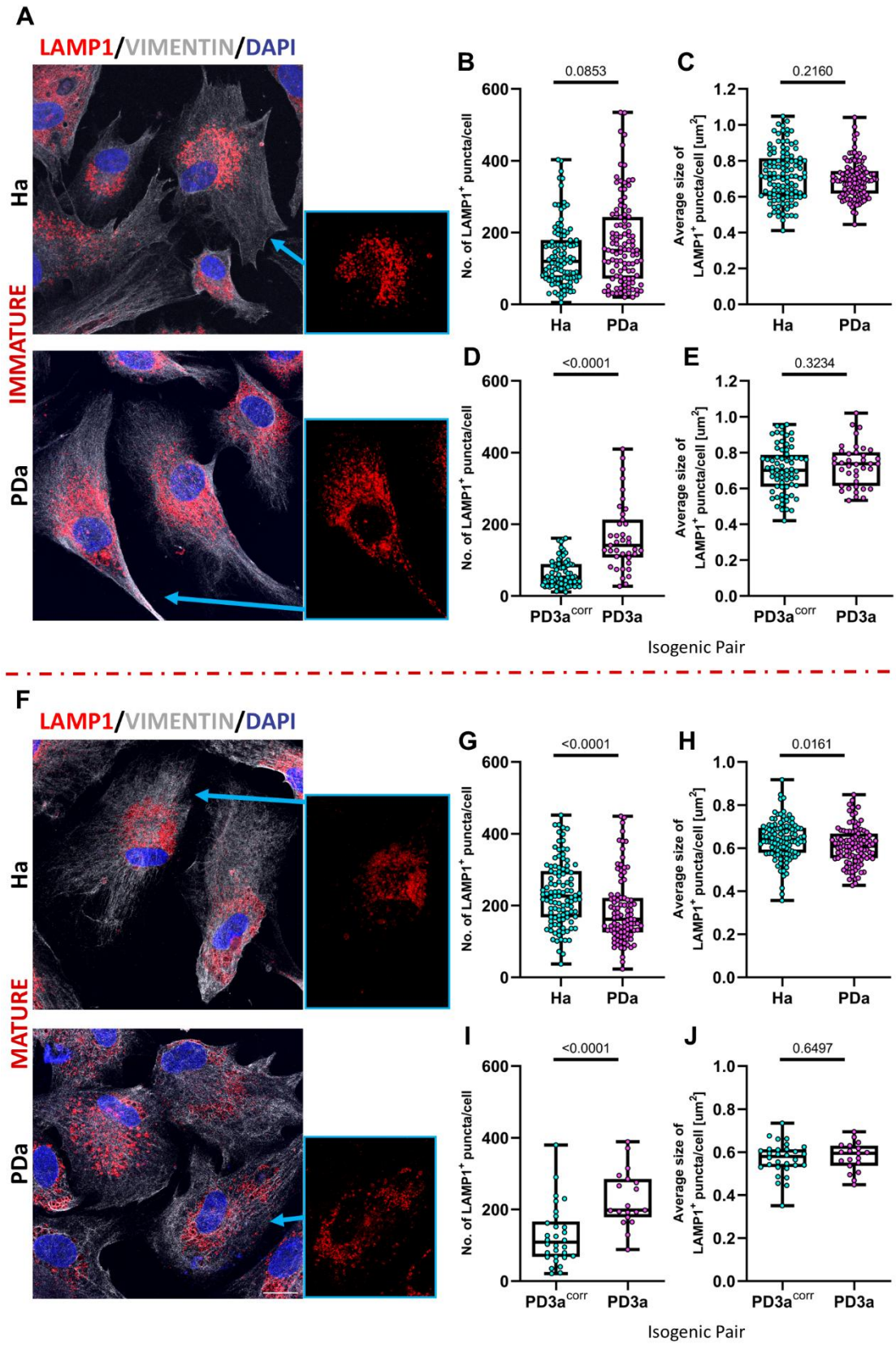

Figure 4. Disturbed lysosomes in the p.A53T-αSyn astrocytes.
A, F: Representative confocal images of immature and mature Ha and PDa immunostained for LAMP1 and VIMENTIN, with DAPI. Insets show LAMP1 staining of the cells marked by arrows. Scale bar: 20 µm. B-E, G-J: Box and whiskers plots showing the distribution of the number of LAMP1$^+$ puncta in non-isogenic (B, G) and isogenic lines (D, I) and of the average size of LAMP1$^+$ puncta in non-isogenic (C, H)

and isogenic lines (E, J) in immature and mature astrocytes, respectively. Data are presented as median with interquartile range and min and max values, and each dot represents a cell. Unpaired t-test with Welch's correction was used for comparisons in E, H, and J. Mann-Whitney test was used for comparisons in B, C, D, G, and I. P-values are shown on the graphs. Sample sizes: B: n = 104 Ha and n = 106 PDa across 4 non-isogenic Ha lines and 4 non-isogenic PDa lines, C: n = 111 Ha and n = 107 PDa across 4 non-isogenic Ha lines and 4 non-isogenic PDa lines, D: n = 67 $PD3a^{corr}$ and n = 39 PD3a, E: n = 68 $PD3a^{corr}$ and n = 39 PD3a, G: n = 107 Ha and n = 94 PDa across 4 non-isogenic Ha lines and 4 non-isogenic PDa lines, H: n = 107 Ha and n = 103 PDa across 4 non-isogenic Ha lines and 4 non-isogenic PDa lines, I,J: n = 30 $PD3a^{corr}$ and n = 19 PD3a.
LAMP1: Lysosome-associated membrane protein 1, Vimentin: Intermediate Filament Protein, DAPI: 4',6-diamidino-2-phenylindole, Ha: healthy astrocytes, PDa: p.A53T-αSyn astrocytes, PD3a: p.A53T-αSyn astrocytes, $PD3a^{corr}$: Corrected isogenic astrocytes

When we assessed mature PDa, we noted that in the isogenic pair the number of $LAMP1^+$ puncta was increased **(Figure 4I)**, as compared to controls, in agreement with the immature astrocytes. However, in the non-isogenic lines the number of $LAMP1^+$ puncta was decreased in PDa, compared to Ha **(Figure 4G)**. Both these results are statistically significant, therefore the differences observed seem ambiguous. In the isogenic pair, the sample size used in this analysis was relatively small (n = 30 Ha and n = 19 PDa) compared to the non-isogenic lines (G: n = 107 Ha and n = 94 PDa), likely explaining the discrepancy. In any case, more in-depth analysis is necessary. With regard to the size of $LAMP1^+$ puncta, we did not observe any differences between mature Ha and PDa, either in the non-isogenic nor in the isogenic lines **(Figure 4H, J)**, in agreement with the results from the immature astrocytes.

<u>Assessment of LAMP1/TOMM20 colocalization as a proxy for mitophagy</u>

We next proceeded with the assessment of the colocalization between LAMP1 and TOMM20, to investigate possible interactions between lysosomes and mitochondria, mostly attributed to mitophagy. In immature PDa the colocalization between LAMP1 and TOMM20 was significantly higher compared to the healthy controls in both non-isogenic and isogenic lines **(Figure 5A-C)**, with the isogenic pair portraying a more intense difference between Ha and PDa. Specifically, by utilizing Manders' coefficient M1, we calculated the area of TOMM20, which corresponds to mitochondria, covered by the $LAMP1^+$ lysosomes. This increase in colocalization likely indicates increased mitophagy.

Interestingly, we obtained different results between immature and mature astrocytes. In mature PDa the colocalization between LAMP1 and TOMM20 was significantly decreased compared to the healthy controls in both non-isogenic and isogenic lines, likely indicating decreased mitophagy **(Figure 5D-F)**. Recurrently, the difference in colocalization between Ha and PDa in the isogenic pair was more intense compared to the non-isogenic lines.

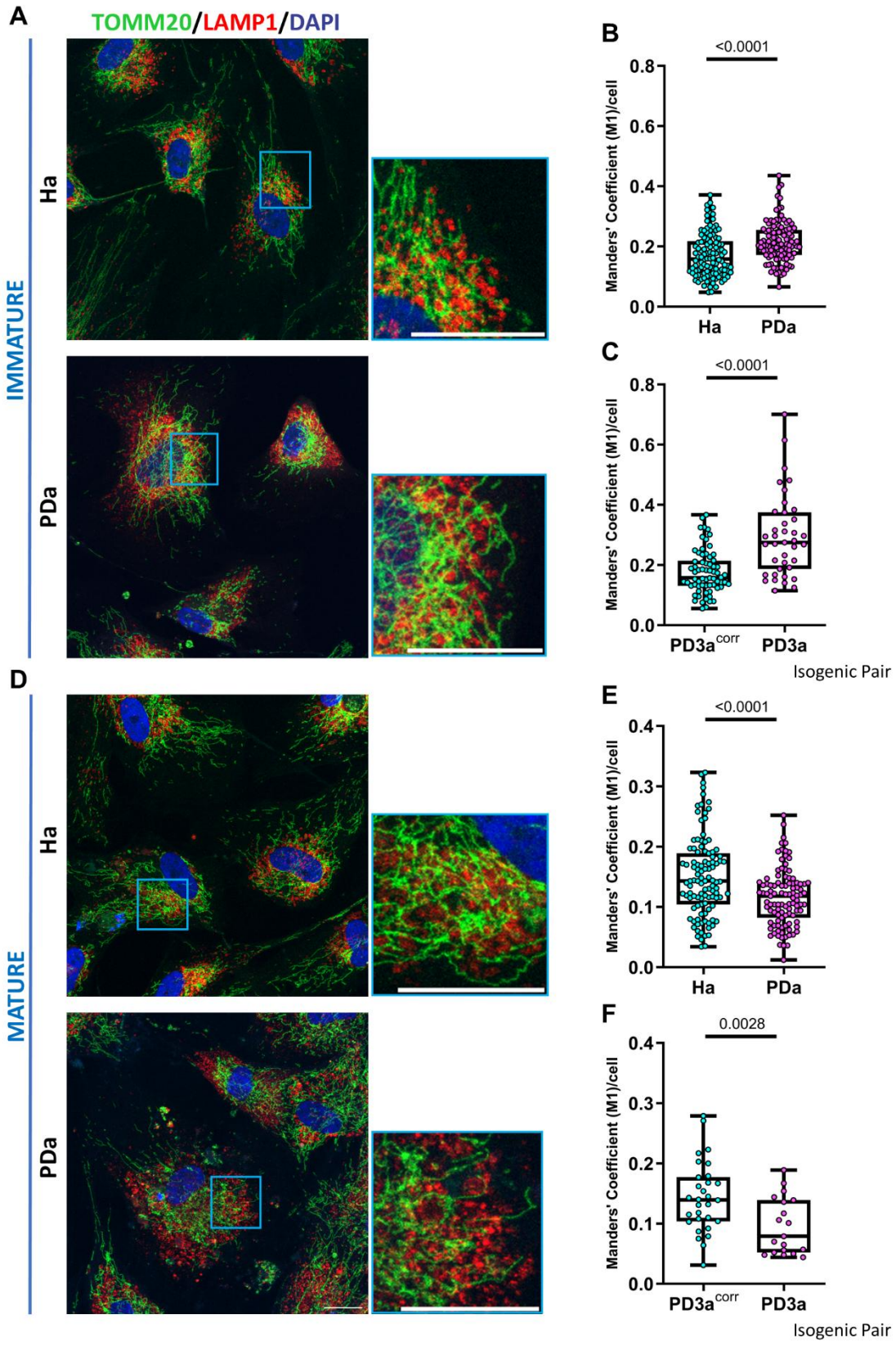

Figure 5. Indications for impaired mitophagy in the p.A53T-αSyn astrocytes.
A, D: Representative confocal images of immature and mature Ha and PDa immunostained for TOMM20 and LAMP1, with DAPI. Insets show magnified views of boxed regions. Scale bar: 20 μm.
B, C, E, F: Box and whiskers plots showing Manders' coefficient M1 indicative of the colocalization between TOMM20 and LAMP1 in non-isogenic (B, E) and isogenic lines (C, F) in immature and mature

astrocytes, respectively. Data are presented as median with interquartile range and min and max values, and each dot represents a cell. Unpaired t-test with Welch's correction was used for comparisons in E and F. Mann-Whitney test was used for comparisons in B and C. P-values are shown on the graphs. Sample sizes: B: n = 110 Ha and n = 107 PDa across 4 non-isogenic Ha lines and 4 non-isogenic PDa lines, C: n = 68 PD3a^{corr} and n = 39 PD3a, E: n = 107 Ha and n = 103 PDa across 4 non-isogenic Ha lines and 4 non-isogenic PDa lines, F: n = 30 PD3a^{corr} and n = 19 PD3a.
TOMM20: Translocase of Outer Mitochondrial Membrane 20, LAMP1: Lysosome-associated membrane protein 1, DAPI: 4',6-diamidino-2-phenylindole, Ha: healthy astrocytes, PDa: p.A53T-αSyn astrocytes, PD3a: p.A53T-αSyn astrocytes, PD3a^{corr}: Corrected isogenic astrocytes

What is worth mentioning is that in immature and mature Ha of both lines the levels of colocalization between the two proteins are very similar (immature Ha: 0.1585 – immature PD3a^{corr}: 0.1580 – mature Ha: 0.143 – mature PD3a^{corr}: 0.1395). Therefore, the difference in colocalization/mitophagy between immature and mature astrocytes is attributed to PDa. Therefore, the combination of the developmental stage of astrocytes with the p.A53T mutation likely affects mitophagy.

p.A53T-αSyn astrocytes show a trend for elevated ROS levels

Previously, we showed that p.A53T-αSyn astrocytes display a trend for increased cytotoxicity **(Figure 1)** and a pattern of mitochondrial fragmentation **(Figure 2)**. Fragmented mitochondria have been associated with high levels of ROS [65]. Previous studies have shown that PD astrocytes, which carry the *LRRK2^{G2019S}* mutation and demonstrate mitochondrial fragmentation, contain higher amounts of oxidized proteins compared to the healthy controls [45]. Furthermore, mutant p.A53T SH-SY5Y cells and iPSC-derived p.A53T-PD neurons exhibit increased mitochondrial oxidative stress [66,67]. Therefore, we next investigated whether the increased cytotoxicity and mitochondrial dysfunction are connected with the presence of ROS in our p.A53T-αSyn astrocytes. We used vital dyes to label ROS (DCFDA), and mitochondrial ROS specifically (Mitotracker Red CMXROS), in both non-isogenic and isogenic lines, and measured fluorescence intensity after live imaging. We observed a trend for elevated total ROS levels in immature PDa compared to their controls **(Figure 6A-C)**, but only the isogenic pair reached statistical significance **(Figure 6C)**. However, this increase was not attributed to the mitochondria, since we did not detect significant differences in the mitochondrial ROS levels between PDa and their controls in either the non-isogenic or the isogenic lines **(Figure 6D-F)**.

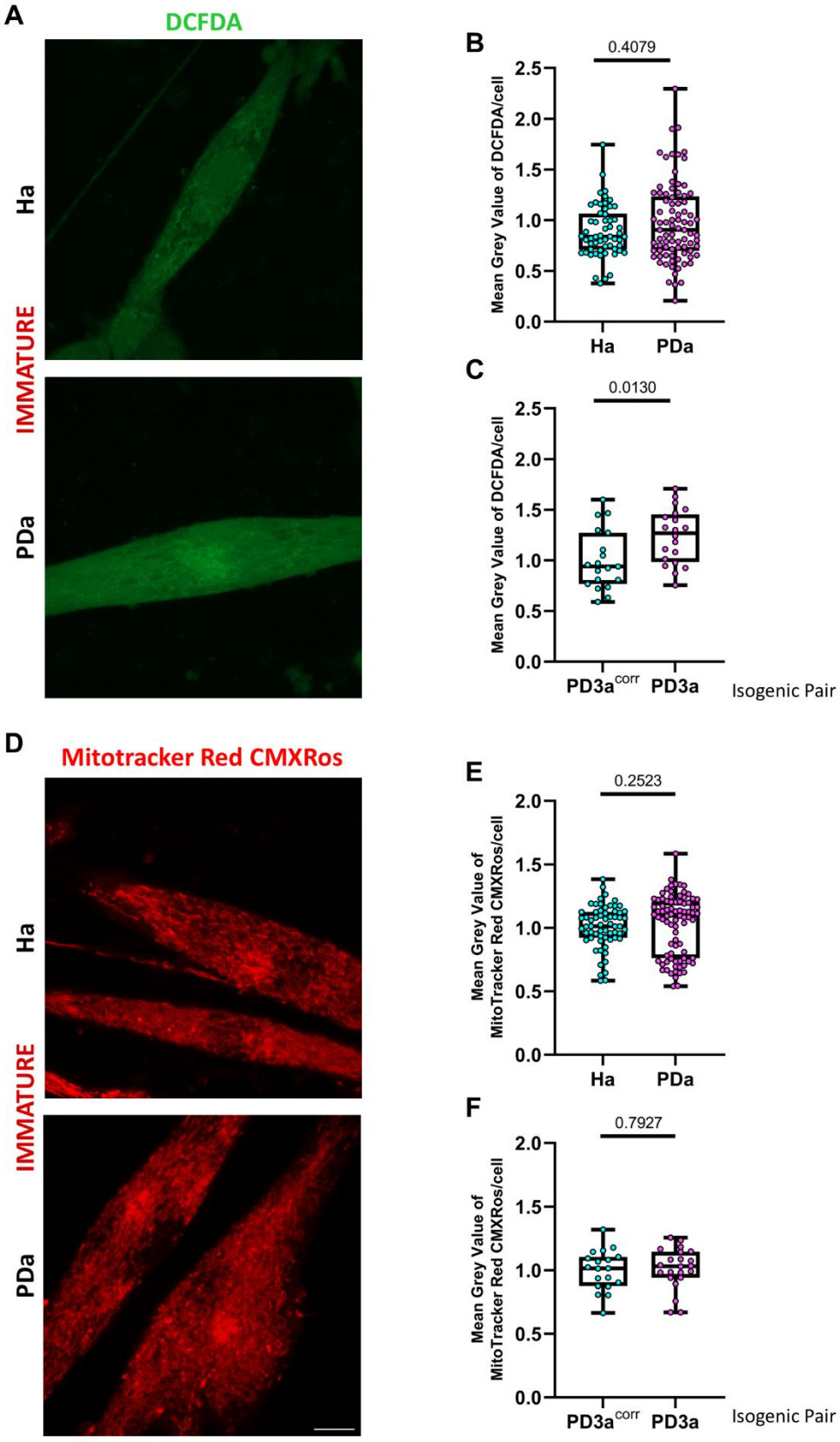

Figure 6. A trend for elevated ROS levels displayed in the p.A53T-αSyn astrocytes.
A, D: Representative live microscopy images of immature Ha and PDa stained for DCFDA, a vital ROS dye and Mitotracker Red CMXRos, a vital mitochondrial ROS dye. Scale bar: 10 μm.
B, C, E, F: Box and whiskers plots showing mean grey value of DCFDA in non-isogenic (B) and isogenic lines (C) and of Mitotracker Red CMXRos in non-isogenic (E) and isogenic lines (F). Data are presented

as median with interquartile range and min and max values, and each dot represents a cell. Unpaired t-test with Welch's correction was used for comparisons in C and F. Mann-Whitney test was used for comparisons in B and E. P-values are shown on the graphs. Sample sizes: B: n = 63 Ha and n = 83 PDa across 3 non-isogenic Ha lines and 4 non-isogenic PDa lines, C: n = 68 PD3a^{corr} and n = 39 PD3a, E: n = 57 Ha and n = 84 PDa across 3 non-isogenic Ha lines and 4 non-isogenic PDa lines, F: n = 19 PD3a^{corr} and n = 22 PD3a.
DCFDA: dichlorodihydrofluorescein diacetate, Ha: healthy astrocytes, PDa: p.A53T-αSyn astrocytes, PD3a: p.A53T-αSyn astrocytes, PD3a^{corr}: Corrected isogenic astrocytes

p.A53T-αSyn astrocytes accumulate lipid droplets

Lipid droplets (LD) are mostly considered as lipid storage organelles, have a unique architecture consisting of a hydrophobic core of neutral lipids, enclosed by a phospholipid monolayer decorated by a specific set of proteins, and are at the center of lipid and energy homeostasis [68]. Recently, it has been proposed that metabolic and hypoxic stressors, which are present in various CNS pathologies, promote LD accumulation in astrocytes [69]. In addition, ROS and neuronal mitochondrial dysfunction lead to accumulation of LD in glia, further promoting neurodegeneration [70]. On the other hand, it has been shown that lipids within astrocytic LD are catabolized by mitochondrial β-oxidation, effectively removing toxic lipid peroxidation products thereby reducing ROS in astrocytes [40]. This process has a protective role, since inhibition of glial LD formation leaves neurons and glia susceptible to damage [70]. Considering these data, along with our results that indicate mitochondrial abnormalities **(Figure 2)** and increased ROS levels **(Figure 6)** in the p.A53T-αSyn astrocytes, we sought to explore if and how the p.A53T mutation affects LD. For this purpose, we stained with Nile Red, a lipophilic dye that stains intracellular LD.

Our results revealed an accumulation of LD in p.A53T-αSyn astrocytes **(Figure 7)**. Specifically, the cell area covered by LD is significantly increased in PDa in both isogenic and non-isogenic lines **(Figure 7A, B, E)**. In addition, p.A53T-αSyn astrocytes compared to their controls showed a trend for increase in the number of LD without reaching significance **(Figure 7A, C, F)**. Moreover, the size of LD is larger in PDa compared to healthy controls, though reaching statistical significance only in the isogenic pair **(Figure 7A, D, G)**. Therefore, our data suggest that astrocytic mitochondrial dysfunction and increased ROS levels impair lipid metabolism, leading to the accumulation of LD.

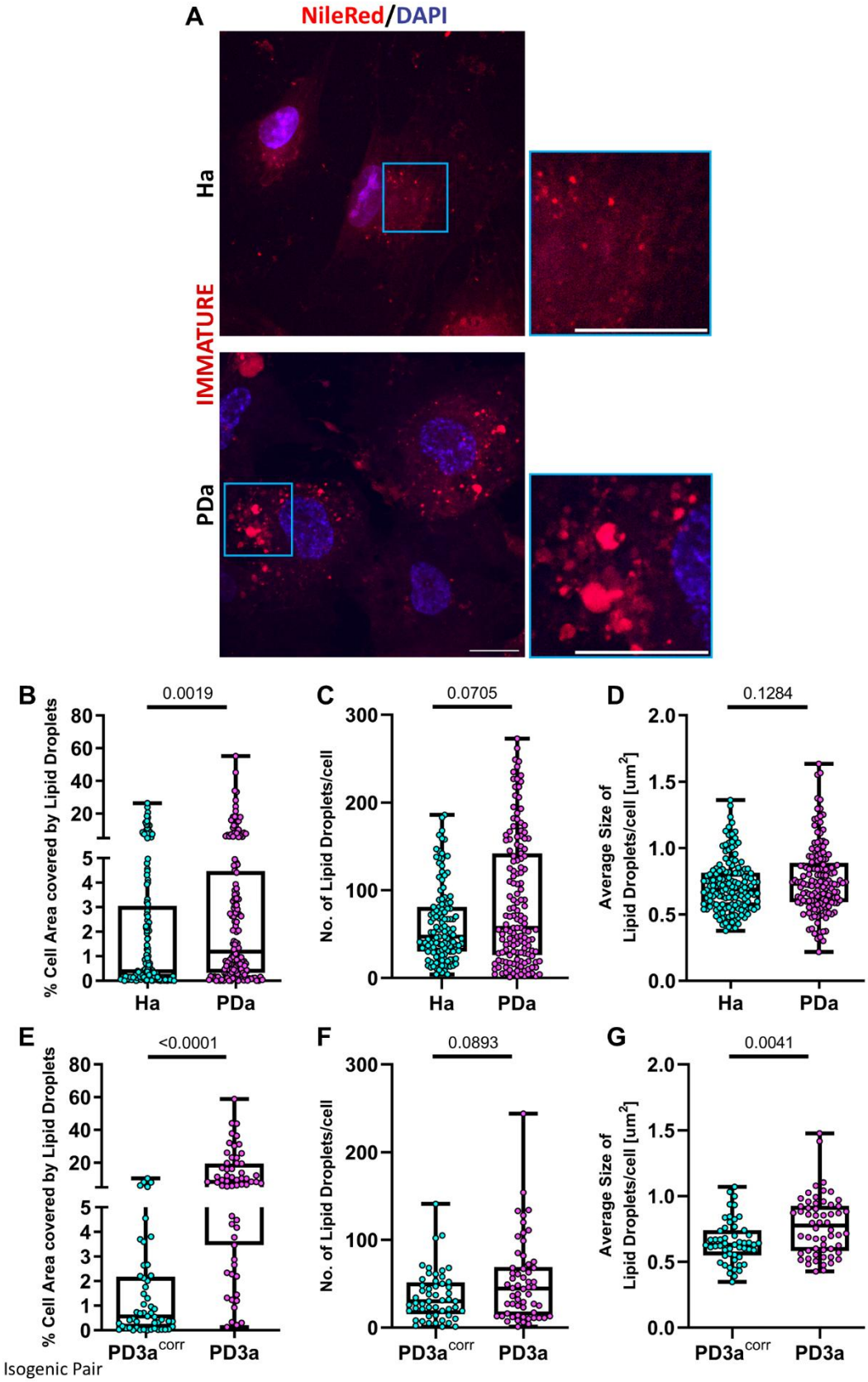

Figure 7. Accumulation of lipid droplets in the p.A53T-αSyn astrocytes.
A: Representative confocal images of immature Ha and PDa live stained with Nile Red, a lipophilic dye. Insets show magnified views of boxed regions. Scale bar: 20 µm.
B-G: Box and whiskers plots showing the distribution of the cell area covered by lipid droplets in non-isogenic (B) and isogenic lines (E), of the number of lipid droplets in non-isogenic (C) and isogenic lines

(F) and of the average size of lipid droplets in non-isogenic (D) and isogenic lines (G). Data are presented as median with interquartile range and min and max values, and each dot represents a cell. Mann-Whitney tests were used for comparisons and p-values are shown on the graphs. Sample sizes: B, D: n = 148 Ha and n = 152 PDa across 4 non-isogenic Ha lines and 4 non-isogenic PDa lines, C: n = 127 Ha and n = 147 PDa across 4 non-isogenic Ha lines and 4 non-isogenic PDa lines, E: n = 52 PD3a^{corr} and n = 59 PD3a, F, G: n = 52 PD3a^{corr} and n = 58 PD3a.
Ha: healthy astrocytes, PDa: p.A53T-αSyn astrocytes, PD3a: p.A53T-αSyn astrocytes, PD3a^{corr}: Corrected isogenic astrocytes

Discussion

By leveraging PD patient-derived iPSCs, this study demonstrates that the p.A53T-αSyn mutation in astrocytes induces a trend for increased cytotoxicity and elevated ROS levels. Moreover, our results indicate an atypical mitochondrial morphology, reflected by a fragmented pattern, and accompanied by indications for impaired mitophagy in the p.A53T-αSyn astrocytes. In addition, we observed lipid droplet accumulation, likely related with disturbances in lipid metabolism.

Research in PD has traditionally focused on neuron-intrinsic deficits, since accumulation of neurotoxic αSyn-rich inclusions results in gradual loss of dopaminergic neurons [1]. Even though astrocytes' involvement in PD has gained ground the last years [25,27], there are limited data about the effect of αSyn mutation particularly on astrocytic mitochondrial function and metabolism. In neurons though, there has been extensive research of how p.A53T-αSyn affects mitochondria and metabolism.

Specifically, p.A53T-αSyn-transfected human-derived neurons exhibited a significant decrease in mitochondrial size, in a dose dependent manner [71]. Furthermore, mutant *SNCA* hiPSC- and human embryonic stem cells, hESC- derived neurons displayed fragmented mitochondria with decreased diameter [72]. In addition, in p.A53T-αSyn iPSC-derived neurons mitochondrial dysfunctions cause an increase in cell death rate [66,67]. These data are in accordance with the results we observed in the p.A53T-αSyn astrocytes, which displayed a trend for increased LDH release **(Figure 1)** and increased mitochondrial fragmentation **(Figure 2**, **Figure 3)**. Disrupted mitochondrial morphology is also in agreement with the comparative proteomic analysis between PDa and Ha, which revealed significant downregulation of TOMM40 and TOMM70 in PDa, two translocases found in the outer mitochondrial membrane (unpublished data). As already mentioned, it is likely that this mitochondrial dysregulation is the result of increased fission or reduced fusion [59]. In addition, mitochondrial fragmentation observed in PDa, likely due to increased fission, may explain the elevated LDH levels, since mitochondrial fission is an early event in cell death [73,74]. Therefore, we suggest that astrocytic mitochondrial fragmentation, caused by the p.A53T-αSyn mutation, leads to increased cytotoxicity. However, more analysis should be performed to find the mechanism this happens.

Under normal conditions, the cells can protect themselves from accumulation of fragmented and thereby dysfunctional mitochondria, and maintain their homeostasis

through the process of autophagy and specifically mitophagy [61]. A first step to elucidate the condition of mitophagy in PD was to study the lysosomes, since mitophagy is a lysosome-dependent pathway. In our study **(Figure 4)** the increase of lysosomes in immature PDa (and isogenic mature PDa) can be translated in different ways. It may reflect reduced consumption of lysosomes due to impaired autophagy or mitophagy, or a compensatory response of lysosomal biogenesis to lysosomal dysfunction [75]. This scenario is also in agreement with our lab results (Paschou, Apokotou et al., under submission), in which a significant decrease of lysosomal enzyme activity and lysosomal acidity were observed, indicating a disrupted environment for the lysosomal enzymes to function properly. Moreover, the majority of mitochondrial fission events (>80%) is marked by LAMP1$^+$ vesicles [76], so the increase in LAMP1$^+$ lysosomes may explain the increased mitochondrial fragmentation **(Figure 2)**.

On the other hand, the elevated LAMP1$^+$ lysosomes in PDa may meet different cellular demands, such as induced mitophagy due to mitochondrial fragmentation and dysfunction [77]. This finding is also in accordance with the increased colocalization between TOMM20 and LAMP1 **(Figure 5A-C)**, indicating increased mitophagy. As mentioned, mitochondria in immature PDa become fragmented **(Figure 2)**, and hence they promote their clearance by mitophagy, which operates as a protective mechanism. Similarly, an increase in the rate of mitophagy has been observed in p.A53T hiPSC- and hESC-derived neurons with a αSyn-induced mitochondrial dysfunction [72] and in p.A53T αSyn-overexpressing mice, where αSyn accumulates in mitochondria of dopaminergic neurons [78,79]. However, in any case, excessive mitochondrial removal could be one of the main contributing factors for mitochondrial loss and excessive or prolonged activation of mitophagy may eventually lead to neurodegeneration [72,78]. In our case, we suggest that mitophagy initially plays a protective role against the αSyn-induced mitochondrial dysfunction, but gradually its overactivation may lead to depletion of the mitochondrial pool and disruption of its network. In depth analysis is underway to better clarify these findings.

In mature PDa though the case is the opposite. The colocalization between TOMM20 and LAMP1 is decreased in PDa compared to the controls, indicating a decrease in mitophagy **(Figure 5D-F)**. Even though, mitochondria are fragmented in mature PDa **(Figure 3)**, it seems those cells fail to increase mitophagy to enhance the clearance of their dysfunctional mitochondria. It is known that immature astrocytes support neuronal maturation by synaptogenesis or axon pathfinding, but when they mature, they limit those functions and gain new ones essential for the CNS homeostasis, such as trophic and metabolic support and BBB regulation [53]. However, in pathological conditions, mature astrocytes become "reactive", which disrupts their homeostatic functions, partially contributing to the pathogenesis of diseases [53]. Moreover, the medium used for the differentiation of astrocytes from the immature state to the

mature, contains two cytokines, CNTF and BMP4, which may cause inflammatory activation. In combination with FBS removal [80] the composition of the maturation medium may induce stress to the differentiating cells, probably leading to "reactive" astrocytes. In addition, we have shown that immature p.A53T-αSyn astrocytes display accumulation of αSyn aggregates and disrupted autophagy, which complicates their clearance (Paschou, Apokotou et al., under submission). This may contribute to overabundance of αSyn aggregates as they develop and reach the mature state. Therefore, we speculate that mature PDa perform diminished mitophagy, as a combination of the developmental stage with the induced stress from the αSyn aggregates and the differentiation medium.

This difference in mitophagy between the two developmental stages of astrocytes is very interesting, since in immature PDa the overactivation of mitophagy leads to astrocytes' dysfunction, while in mature astrocytes insufficient mitophagy leads to accumulation of disrupted mitochondria and in due course to astrocytic deregulations. It seems like the p.A53T mutation acts differently on astrocytic mitophagy, depending on their state. We propose that in both developmental stages, the interaction between PINK1 and Parkin, or their protein levels, may contribute to mitophagy impairment. Mitophagy is a crucial pathway mediated by PINK1 and Parkin, in which PINK1 accumulates on the outer membrane of damaged mitochondria, recruiting Parkin to facilitate autophagosome formation and subsequent mitochondrial degradation [81]. Dysregulation of this pathway has been linked to PD, as impaired mitophagy may exacerbate mitochondrial dysfunction, a hallmark of PD [82]. Additionally, this dysfunction may promote the aggregation of αSyn, another key pathological feature of PD, thereby connecting PINK1-Parkin activity with αSyn pathology [83].

Oxidative stress is an important pathogenic factor in PD. Mitochondria are a major source of ROS in cells as a byproduct of the electron transport chain activity and damaged mitochondria induce oxidative stress, which is a well-known contributor to neurodegeneration [38]. In addition, astrocytes play a key role in controlling redox homeostasis in the brain, especially since neurons display limited defense mechanisms against oxidative stress compared to astrocytes [84]. However, when astrocytes are compromised themselves, they cannot perform detox processes. In our lab, preliminary Seahorse analysis on PD astrocytes demonstrated dysfunctions in the electron transport chain activity, since PDa displayed reduced oxygen consumption rate and ATP production (not shown). Furthermore, we showed that mitochondria are disrupted **(Figure 2)**. These data combined give us a hint of probable increased ROS levels, which was proved by our results **(Figure 6A-C)**, but was not attributed to mitochondria **(Figure 6D-F)**. Probably in our case, the origin of the elevated total ROS levels differs. On the other hand, mitochondria might be the cause of these increased ROS levels, indirectly. ROS occur mainly at complexes I and III of the respiratory chain,

when the electron transport chain is compromised, leading to a leakage of electrons, which react with oxygen to form superoxide [38]. Furthermore, it has been shown that iPSC-derived astrocytes from PD-patients carrying the *LRRK2*^{G2019S} mutation and p.A53T neurons display reduced mitochondrial membrane potential [45,72], which may affect the membrane's permeability. Therefore, ROS may be produced in mitochondria, but they may disperse in the cell due to probable high mitochondrial membrane permeability. Either way we suggest that elevated total ROS levels contribute to astrocytic deregulation, either originating from mitochondria indirectly or from other cell compartments.

Astrocytic mitochondria play an important role in energy metabolism and specifically in fatty acid metabolism [85]. However, disrupted mitochondria [70] and ROS [86] can alter this metabolism, thereby promoting neurodegeneration. Fatty acid metabolism is strongly associated with the accumulation of LD, indicating the condition of it. Accumulation of LD may have a protective role against lipotoxicity [40,70] or may contribute further to neuropathology [69]. Our data suggest that the increased accumulation of LD in immature PDa **(Figure 7)** is correlated with impaired astrocytic lipid metabolism, which is supported by the presence of fragmented mitochondria **(Figure 2)** and increased ROS levels **(Figure 6)**. This is also supported by the proteomic analysis performed in PDa in our lab (Paschou, Apokotou et al., under submission). This analysis demonstrated upregulation of VLDL receptor, which promotes an increase in number and size of LD and ultimately lipotoxicity [87] and of HSD17B11, which induces LD aggregation [88]. In addition, the proteomic analysis revealed a significant downregulation of PIP4K2A, an enzyme which generates PI-4,5-P_2, which regulates peroxisomal fatty acid oxidation by mediating trafficking of LD to peroxisomes and thereby reducing LD aggregation.

Considering everything, our results indicate that PD astrocytes exhibit problematic mitochondrial morphology and function, as well as disrupted lipid metabolism. The main role of astrocytes is to support neurons and therefore, we suggest that astrocytes' dysfunctions affect neurons, thereby contributing to the neuropathology of PD. However, further in-depth analyses are underway to confirm our suggestion.

Acknowledgments

Firstly, I would like to express my deepest gratitude to my supervisor, Dr Florentia Papastefanaki, for giving me the opportunity to perform my master's thesis in the laboratory and for her constant advice, support, ideas, help and patience during this year. Next, I would like to thank my Stem-Cell lab partners, Anastasios Kollias, Christina Paschou and Olympia Apokotou whom their help, advice and support was unconditional and my fellow students Sofia Dede, Constantinos Sideris and Eirini Dima. Furthermore, I would like to thank Dr Rebecca Matsas for hosting me in the lab and Dr Era Taoufik and her group for providing me with their company, their practical

suggestions, and for always being willing to answer any question that I might had. During my thesis, I had the pleasure of working and communicating with all the members of the laboratory, both from our group and from Dimitra Thomaidou's and Maria Gaitanou's groups. Lastly, I would be remiss in not mentioning my family and friends for all the encouragement and emotional support.

The research project was supported by the Hellenic Foundation for Research and Innovation (H.F.R.I.) under the "1st Call for H.F.R.I. Research Projects to support Faculty members and Researchers and the procurement of high-cost research equipment" (Project 1019-DiseasePhenoTarget; PI: R. Matsas) & by the General Secretariat for Research and Innovation under the action "National research network to elucidate the genetic basis of Alzheimer's and Parkinson's.

No plagiarism statement

The Authors confirm that intact sentences or paragraphs from other publications are not included and that there is no significant overlap with other publications.

References

1. Poewe, W. *et al.* Parkinson disease. *Nat Rev Dis Primers* **3**, 1–21 (2017).
2. Pang, S. Y. Y. *et al.* The interplay of aging, genetics and environmental factors in the pathogenesis of Parkinson's disease. *Transl Neurodegener* **8**, (2019).
3. Del Rey, N. L. G. *et al.* Advances in parkinson's disease: 200 years later. *Front Neuroanat* **12**, (2018).
4. Ascherio, A. & Schwarzschild, M. A. The epidemiology of Parkinson's disease: risk factors and prevention. *Lancet Neurol* **15**, 1257–1272 (2016).
5. Zimprich, A. *et al.* Mutations in LRRK2 cause autosomal-dominant parkinsonism with pleomorphic pathology. *Neuron* **44**, 601–607 (2004).
6. Paisán-Ruíz, C. *et al.* Cloning of the gene containing mutations that cause PARK8-linked Parkinson's disease. *Neuron* **44**, 595–600 (2004).
7. Lücking, C. B. *et al.* Association between early-onset Parkinson's disease and mutations in the parkin gene. *N Engl J Med* **342**, 1560–1567 (2000).
8. Smith, L. & Schapira, A. H. V. GBA Variants and Parkinson Disease: Mechanisms and Treatments. *Cells* **11**, 1261 (2022).
9. Bonifati, V. *et al.* Mutations in the DJ-1 gene associated with autosomal recessive early-onset parkinsonism. *Science (1979)* **299**, 256–259 (2003).
10. Polymeropoulos, M. H. *et al.* Mutation in the alpha-synuclein gene identified in families with Parkinson's disease. *Science (1979)* **276**, 2045–2047 (1997).
11. Krüger, R. *et al.* Ala30Pro mutation in the gene encoding alpha-synuclein in Parkinson's disease. *Nat Genet* **18**, 106–108 (1998).

12. Kahle, P. J. *et al.* Subcellular Localization of Wild-Type and Parkinson's Disease-Associated Mutant α-Synuclein in Human and Transgenic Mouse Brain. *Journal of Neuroscience* **20**, 6365–6373 (2000).

13. Lee, S. J., Jeon, H. & Kandror, K. V. Alpha-synuclein is localized in a subpopulation of rat brain synaptic vesicles. *Acta Neurobiol Exp (Wars)* **68**, 509–515 (2008).

14. Murphy, D. D., Rueter, S. M., Trojanowski, J. Q. & Lee, V. M. Y. Synucleins are developmentally expressed, and alpha-synuclein regulates the size of the presynaptic vesicular pool in primary hippocampal neurons. *J Neurosci* **20**, 3214–3220 (2000).

15. Cabin, D. E. *et al.* Synaptic vesicle depletion correlates with attenuated synaptic responses to prolonged repetitive stimulation in mice lacking alpha-synuclein. *J Neurosci* **22**, 8797–8807 (2002).

16. Lashuel, H. A., Overk, C. R., Oueslati, A. & Masliah, E. The many faces of α-synuclein: from structure and toxicity to therapeutic target. *Nat Rev Neurosci* **14**, 38–48 (2013).

17. Burré, J. *et al.* Alpha-synuclein promotes SNARE-complex assembly in vivo and in vitro. *Science (1979)* **329**, 1663–1667 (2010).

18. Kragh, C. L., Ubhi, K., Wyss-Corey, T. & Masliah, E. Autophagy in Dementias. *Brain Pathology* **22**, 99 (2011).

19. Conway, K. A., Harper, J. D. & Lansbury, P. T. Accelerated in vitro fibril formation by a mutant α-synuclein linked to early-onset Parkinson disease. *Nat Med* **4**, 1318–1320 (1998).

20. Braak, H. *et al.* Staging of brain pathology related to sporadic Parkinson's disease. *Neurobiol Aging* **24**, 197–211 (2003).

21. Spillantini, M. G. *et al.* α-Synuclein in Lewy bodies. *Nature* **388**, 839–840 (1997).

22. Braak, H., Sastre, M. & Del Tredici, K. Development of alpha-synuclein immunoreactive astrocytes in the forebrain parallels stages of intraneuronal pathology in sporadic Parkinson's disease. *Acta Neuropathol* **114**, 231–241 (2007).

23. Sorrentino, Z. A., Giasson, B. I. & Chakrabarty, P. α-Synuclein and astrocytes: tracing the pathways from homeostasis to neurodegeneration in Lewy body disease. *Acta Neuropathol* **138**, (2019).

24. Wakabayashi, K., Hayashi, S., Yoshimoto, M., Kudo, H. & Takahashi, H. NACP/alpha-synuclein-positive filamentous inclusions in astrocytes and oligodendrocytes of Parkinson's disease brains. *Acta Neuropathol* **99**, 14–20 (2000).

25. Booth, H. D. E., Hirst, W. D. & Wade-Martins, R. The Role of Astrocyte Dysfunction in Parkinson's Disease Pathogenesis. *Trends in Neurosciences* **40**, 358–370 (2017).

26. Rostami, J. *et al.* Human Astrocytes Transfer Aggregated Alpha-Synuclein via Tunneling Nanotubes. *J Neurosci* **37**, 11835–11853 (2017).

27. Brandebura, A. N., Paumier, A., Onur, T. S. & Allen, N. J. Astrocyte contribution to dysfunction, risk and progression in neurodegenerative disorders. *Nat Rev Neurosci* **24**, 23–39 (2023).

28. Bushong, E. A., Martone, M. E., Jones, Y. Z. & Ellisman, M. H. Protoplasmic astrocytes in CA1 stratum radiatum occupy separate anatomical domains. *J Neurosci* **22**, 183–192 (2002).

29. Gollihue, J. L. & Norris, C. M. Astrocyte mitochondria: Central players and potential therapeutic targets for neurodegenerative diseases and injury. *Ageing Res Rev* **59**, (2020).

30. Mauch, D. H. *et al.* CNS synaptogenesis promoted by glia-derived cholesterol. *Science* **294**, 1354–1357 (2001).

31. Powell, E. M. & Geller, H. M. Dissection of astrocyte-mediated cues in neuronal guidance and process extension . *Glia* **26**, 73–83 (1999).

32. Clarke, L. E. & Barres, B. A. Emerging roles of astrocytes in neural circuit development. *Nat Rev Neurosci* **14**, 311–321 (2013).

33. Chung, W. S. *et al.* Astrocytes mediate synapse elimination through MEGF10 and MERTK pathways. *Nature* **504**, 394–400 (2013).

34. Ullian, E. M., Sapperstein, S. K., Christopherson, K. S. & Barres, B. A. Control of synapse number by glia. *Science* **291**, 657–661 (2001).

35. Liddelow, S. & Barres, B. SnapShot: Astrocytes in Health and Disease. *Cell* **162**, 1170-1170.e1 (2015).

36. Parnis, J. *et al.* Mitochondrial Exchanger NCLX Plays a Major Role in the Intracellular Ca2+ Signaling, Gliotransmission, and Proliferation of Astrocytes. *The Journal of Neuroscience* **33**, 7206 (2013).

37. Abbott, N. J., Rönnbäck, L. & Hansson, E. Astrocyte-endothelial interactions at the blood-brain barrier. *Nat Rev Neurosci* **7**, 41–53 (2006).

38. Bantle, C. M., Hirst, W. D., Weihofen, A. & Shlevkov, E. Mitochondrial Dysfunction in Astrocytes: A Role in Parkinson's Disease? *Front Cell Dev Biol* **8**, (2021).

39. Attwell, D. *et al.* Glial and neuronal control of brain blood flow. *Nature* **468**, 232–243 (2010).

40. Ioannou, M. S. *et al.* Neuron-Astrocyte Metabolic Coupling Protects against Activity-Induced Fatty Acid Toxicity. *Cell* **177**, 1522-1535.e14 (2019).

41. Chan, F., Lax, N. Z., Davies, C. H., Turnbull, D. M. & Cunningham, M. O. Neuronal oscillations: A physiological correlate for targeting mitochondrial dysfunction in neurodegenerative diseases? *Neuropharmacology* **102**, 48–58 (2016).

42. Wang, C., Yang, T., Liang, M., Xie, J. & Song, N. Astrocyte dysfunction in Parkinson's disease: from the perspectives of transmitted α-synuclein and genetic modulation. *Transl Neurodegener* **10**, (2021).

43. Braidy, N. *et al.* Uptake and mitochondrial dysfunction of alpha-synuclein in human astrocytes, cortical neurons and fibroblasts. *Transl Neurodegener* **2**, (2013).

44. Lindström, V. *et al.* Extensive uptake of α-synuclein oligomers in astrocytes results in sustained intracellular deposits and mitochondrial damage. *Mol Cell Neurosci* **82**, 143–156 (2017).

45. Ramos-Gonzalez, P. *et al.* Astrocytic atrophy as a pathological feature of Parkinson's disease with LRRK2 mutation. *NPJ Parkinsons Dis* **7**, (2021).

46. Sonninen, T. M. *et al.* Metabolic alterations in Parkinson's disease astrocytes. *Sci Rep* **10**, (2020).

47. Chen, C. *et al.* Astrocytic Changes in Mitochondrial Oxidative Phosphorylation Protein Levels in Parkinson's Disease. *Movement Disorders* **37**, 302–314 (2022).

48. Kouroupi, G. *et al.* Defective synaptic connectivity and axonal neuropathology in a human iPSC-based model of familial Parkinson's disease. *Proc Natl Acad Sci U S A* **114**, E3679–E3688 (2017).

49. Soldner, F. *et al.* Generation of isogenic pluripotent stem cells differing exclusively at two early onset Parkinson point mutations. *Cell* **146**, 318–331 (2011).

50. Kriks, S. *et al.* Dopamine neurons derived from human ES cells efficiently engraft in animal models of Parkinson's disease. *Nature 2011 480:7378* **480**, 547–551 (2011).

51. de Rus Jacquet, A. Preparation and Co-Culture of iPSC-Derived Dopaminergic Neurons and Astrocytes. *Curr Protoc Cell Biol* **85**, (2019).

52. TCW, J. *et al.* An Efficient Platform for Astrocyte Differentiation from Human Induced Pluripotent Stem Cells. *Stem Cell Reports* **9**, 600–614 (2017).

53. Lattke, M. & Guillemot, F. Understanding astrocyte differentiation: Clinical relevance, technical challenges, and new opportunities in the omics era. *Wires Mechanisms of Disease* **14**, e1557 (2022).

54. Brovkovych, V., Aldrich, A., Li, N., Atilla-Gokcumen, G. E. & Frasor, J. Removal of Serum Lipids and Lipid-Derived Metabolites to Investigate Breast Cancer Cell Biology. *Proteomics* **19**, 1800370 (2019).

55. Chaudhry, A., Shi, R. & Luciani, D. S. A pipeline for multidimensional confocal analysis of mitochondrial morphology, function, and dynamics in pancreatic β-cells. *Am J Physiol Endocrinol Metab* **318**, E87–E101 (2020).

56. Kirshner, H., Aguet, F., Sage, D. & Unser, M. 3-D PSF fitting for fluorescence microscopy: implementation and localization application. *J Microsc* **249**, 13–25 (2013).

57. Dey, N. *et al.* Richardson–Lucy algorithm with total variation regularization for 3D confocal microscope deconvolution. *Microsc Res Tech* **69**, 260–266 (2006).

58. Sage, D. *et al.* DeconvolutionLab2: An open-source software for deconvolution microscopy. *Methods* **115**, 28–41 (2017).

59. Knott, A. B., Perkins, G., Schwarzenbacher, R. & Bossy-Wetzel, E. Mitochondrial fragmentation in neurodegeneration. *Nat Rev Neurosci* **9**, 505–518 (2008).

60. Larsen, N. J., Ambrosi, G., Mullett, S. J., Berman, S. B. & Hinkle, D. A. DJ-1 knock-down impairs astrocyte mitochondrial function. *Neuroscience* **196**, 251–264 (2011).

61. Lemasters, J. J. Selective mitochondrial autophagy, or mitophagy, as a targeted defense against oxidative stress, mitochondrial dysfunction, and aging. *Rejuvenation Res* **8**, 3–5 (2005).

62. Pickles, S., Vigié, P. & Youle, R. J. Mitophagy and Quality Control Mechanisms in Mitochondrial Maintenance. *Current Biology* **28**, R170–R185 (2018).

63. Wong, Y. C., Kim, S., Peng, W. & Krainc, D. Regulation and Function of Mitochondria–Lysosome Membrane Contact Sites in Cellular Homeostasis. *Trends Cell Biol* **29**, 500–513 (2019).

64. Bonam, S. R., Wang, F. & Muller, S. Lysosomes as a therapeutic target. *Nature Reviews Drug Discovery 2019 18:12* **18**, 923–948 (2019).

65. Ježek, J., Cooper, K. F. & Strich, R. Reactive Oxygen Species and Mitochondrial Dynamics: The Yin and Yang of Mitochondrial Dysfunction and Cancer Progression. *Antioxidants (Basel)* **7**, (2018).

66. Hu, D. *et al.* Alpha-synuclein suppresses mitochondrial protease ClpP to trigger mitochondrial oxidative damage and neurotoxicity. *Acta Neuropathol* **137**, (2019).

67. Choi, M. L. *et al.* Pathological structural conversion of α-synuclein at the mitochondria induces neuronal toxicity. *Nat Neurosci* **25**, 1134–1148 (2022).

68. Olzmann, J. A. & Carvalho, P. Dynamics and functions of lipid droplets. *Nature Reviews Molecular Cell Biology 2018 20:3* **20**, 137–155 (2018).

69. Smolič, T. *et al.* Astrocytes in stress accumulate lipid droplets. *Glia* **69**, 1540 (2021).

70. Liu, L. *et al.* Glial lipid droplets and ROS induced by mitochondrial defects promote neurodegeneration. *Cell* **160**, 177–190 (2015).

71. Devoto, V. M. P. *et al.* αsynuclein control of mitochondrial homeostasis in human-derived neurons is disrupted by mutations associated with Parkinson's disease. *Sci Rep* **7**, (2017).

72. Ryan, T. *et al.* Cardiolipin exposure on the outer mitochondrial membrane modulates α-synuclein. *Nat Commun* **9**, (2018).

73. Lee, Y. J., Jeong, S. Y., Karbowski, M., Smith, C. L. & Youle, R. J. Roles of the mammalian mitochondrial fission and fusion mediators Fis1, Drp1, and Opa1 in apoptosis. *Mol Biol Cell* **15**, 5001–5011 (2004).

74. Frank, S. *et al.* The role of dynamin-related protein 1, a mediator of mitochondrial fission, in apoptosis. *Dev Cell* **1**, 515–525 (2001).

75. Mutvei, A. P., Nagiec, M. J. & Blenis, J. Balancing lysosome abundance in health and disease. *Nature Cell Biology 2023 25:9* **25**, 1254–1264 (2023).

76. Wong, Y. C., Ysselstein, D. & Krainc, D. Mitochondria–lysosome contacts regulate mitochondrial fission via RAB7 GTP hydrolysis. *Nature* **554**, 382–386 (2018).

77. Yang, C. & Wang, X. Lysosome biogenesis: Regulation and functions. *Journal of Cell Biology* **220**, (2021).

78. Choubey, V. *et al.* Mutant A53T α-Synuclein induces neuronal death by increasing mitochondrial autophagy. *Journal of Biological Chemistry* **286**, 10814–10824 (2011).

79. Chinta, S. J., Mallajosyula, J. K., Rane, A. & Andersen, J. K. Mitochondrial alpha-synuclein accumulation impairs complex I function in dopaminergic neurons and results in increased mitophagy in vivo. *Neurosci Lett* **486**, 235–239 (2010).

80. Basso, F. G. *et al.* Nutritional deprivation and LPS exposure as feasible methods for induction of cellular — A methodology to validate for vitro photobiomodulation studies. *J Photochem Photobiol B* **159**, 205–210 (2016).

81. Pickrell, A. M. & Youle, R. J. The roles of PINK1, parkin, and mitochondrial fidelity in Parkinson's disease. *Neuron* **85**, 257–273 (2015).

82. Liu, J., Liu, W., Li, R. & Yang, H. Mitophagy in Parkinson's Disease: From Pathogenesis to Treatment. *Cells* **8**, 712 (2019).

83. Kinnart, I. *et al.* Elevated α-synuclein levels inhibit mitophagic flux. *npj Parkinson's Disease 2024 10:1* **10**, 1–15 (2024).

84. Fernandez-Fernandez, S., Almeida, A. & Bolaños, J. P. Antioxidant and bioenergetic coupling between neurons and astrocytes. *Biochem J* **443**, 3–12 (2012).

85. Lee, J. A., Hall, B., Allsop, J., Alqarni, R. & Allen, S. P. Lipid metabolism in astrocytic structure and function. *Seminars in Cell and Developmental Biology* vol. 112 123–136 Preprint at https://doi.org/10.1016/j.semcdb.2020.07.017 (2021).

86. Nemoto, S., Takeda, K., Yu, Z.-X., Ferrans, V. J. & Finkel, T. Role for mitochondrial oxidants as regulators of cellular metabolism. *Mol Cell Biol* **20**, 7311–7318 (2000).

87. Perman, J. C. *et al.* The VLDL receptor promotes lipotoxicity and increases mortality in mice following an acute myocardial infarction. *J Clin Invest* **121**, 2625 (2011).

88. Liu, Y. *et al.* Hydroxysteroid dehydrogenase family proteins on lipid droplets through bacteria, C. elegans, and mammals. *Biochim Biophys Acta Mol Cell Biol Lipids* **1863**, 881–894 (2018).